Experimental Study of the Space-Time Properties of Acoustic Channels for Underwater Communications

Beatrice Tomasi*, Giovanni Zappa‡, Kim McCoy‡, Paolo Casari*, Michele Zorzi*
*Department of Information Engineering, University of Padova, Italy — {tomasibe, casarip, zorzi}@dei.unipd.it
‡NATO Undersea Research Centre (NURC), La Spezia, Italy — {zappa, mccoy}@nurc.nato.int

***Abstract*—In this paper, we present an analysis of the space-time correlation and power-delay profile (PDP) properties of the underwater acoustic channel in the nearabouts of the Pianosa Island, off the north-western coast of Italy. Our data has been collected during sea trials which took place from May to September 2009. Using the results from this evaluation, we compare the measured bit error rates affecting the transmission of Frequency-Hopping Binary Frequency Shift Keying (FH-BFSK) against those obtained by simulating the same digital modulation scheme over synthesized channels whose spread in time has the same statistical properties as those found in the trials, and whose channel taps are Rayleigh-distributed. The results show a generally good accordance of the simulated performance with the outcomes of the experiments.**

Moreover, given the absence of a widely agreed upon underwater channel model, and the recent interest in incorporating more accurate propagation simulators into network simulators, we compare the measured channel impulse responses against those obtained through the ray tracing tool Bellhop, and give some observations about the suitability of the tool for the purpose of reproducing realistic channel traces.

I. Introduction

Underwater acoustic networks are of great interest for both civilian and military applications; however, they still represent a challenge due to the limited bandwidth available for communication and the high amount of time- and space-varying reverberation affecting signals in most scenarios of practical interest. Because of the amount of money and resources required for deployment and maintenance of a test system, simulation is still the most widely employed investigation tool for underwater networks. What still lacks to make up a full-rounded simulator is a widely agreed upon channel model representing the behavior of the underwater channel at least from a statistical point of view. Following similar efforts [1], [2], in this paper we make some steps in this direction by performing an estimation of the space and time correlation, and power-delay profile (PDP) properties of an underwater acoustic channel. Our estimates are derived from a large data set collected during the SubNet 2009 sea trials, which took place from May to September 2009 in waters around Pianosa Island, located in the Tyrrhenian sea, off the north-western coast of Italy (about 42.585°N, 10.1°E).

Broadly speaking, the underwater channel coherence time is the period over which the propagation paths of the acoustic energy and their intensity incur little changes, resulting in approximately stationary channel realizations as seen at the receiver; the power-delay profile (and a measure of its "length", i.e., the channel time spread)[1] represents instead the period over which separately detectable arrivals reach the receiver, and can be measured as the standard deviation of the probability distribution obtained by normalizing the average squared magnitude of the impulse response. A measure of the channel coherence time, as well as of the time spread of the channel response, is of practical importance in many communication-related tasks. For example, when simulating underwater communications, channel realizations (and therefore fading and other channel variability phenomena) are assumed to be approximately stationary within a certain period of time, whose length should be estimated depending on the expected channel coherence time. The latter measure can also help tune signal processing algorithms, e.g., by setting the update period of filter coefficients in adaptive equalizers: the frequency of such updates must be directly dependent on the channel coherence time. Also, when simulating underwater communications, channel estimates are assumed to be stable within a certain time period, whose length should be tuned to the expected channel coherence time.

In this paper, we consider a JANUS version 0.0 waveform [3] transmitted in the 9–14 kHz band. In particular we focus on the wideband hyperbolic frequency modulated (HFM) sine wave portion within the JANUS signal preamble: such signal has a very narrow autocorrelation function, which provides fine resolution in the computation of the channel responses at the output of a filter matched to the waveform. Based on this output, we estimate the PDP and the time correlation function of the channel. Similar evaluations of the channel coherence have been conducted in the past [4]–[7], at various frequencies and using different kinds of probe signals. Unlike most previous work, our data set contains data gathered over a period of three months, which allows to draw conclusions on the long-term stability of channel parameters and PDPs. We also give a measure of spatial channel coherence across the three receivers of the vertical hydrophone array, and compare the measured channel impulse responses against those obtained by simulating channel propagation through the Bellhop ray tracing tool [8].

We finally study the Bit Error Rate (BER) of the Frequency-Hopping Binary Frequency-Shift Keying (FH-BFSK) modulation used for the JANUS signals versus the Signal to Noise

[1] In the following, we will use the terms time spread and delay spread interchangeably

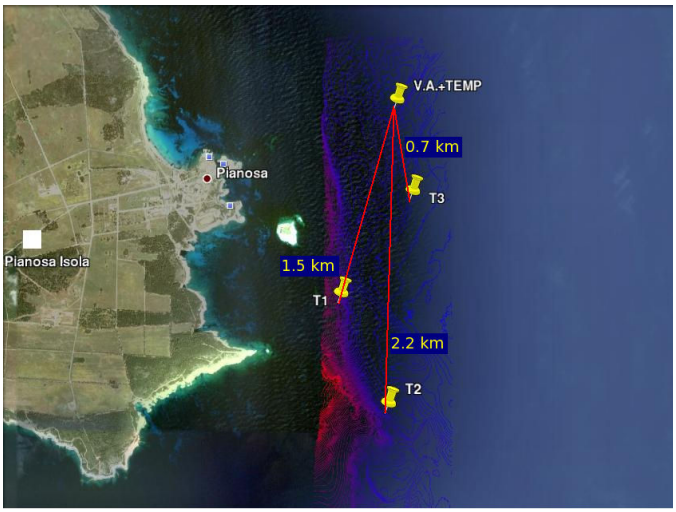

Figure 1. A scheme of the testbed deployment off the coast of the Pianosa Island.

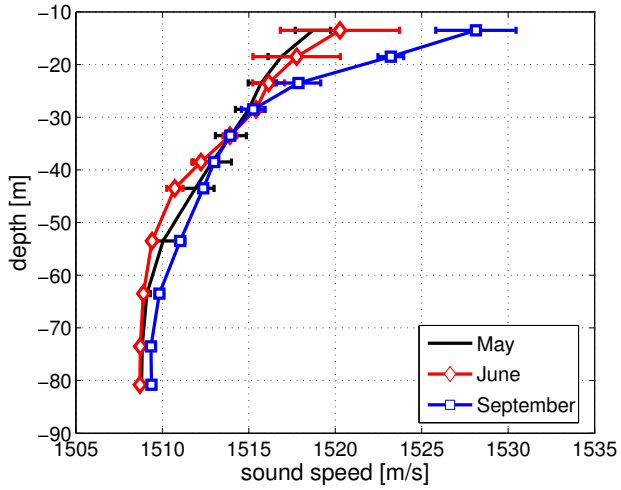

Figure 2. Average and standard deviation of SSP during experiments on May 30, June 5 and September 2.

Ratio (SNR) measured for each transmission, and compare this against curves obtained by Monte-Carlo simulation of the same modulation over a tapped delay line channel where the amplitude of the taps is Rayleigh distributed and the delay spread of the channel response is set according to the measured data. In simulations, we assume Additive White Gaussian Noise (AWGN).[2] This evaluation highlights the main factors behind the performance of JANUS transmissions over typical summer shallow-water channel profiles.

II. Experimental Testbed Setup

The SubNet 2009 sea trials took place off the eastern shore of the Pianosa Island, Italy (42.585°N, 10.1°E). The experimental testbed consisted of one vertical array (VA) of four hydrophones moored at different depths, and three acoustic transmitters (Teledyne-Low Frequency modems [9]) placed on a tripod on the sea floor at different distances from the VA (700 m, 1500 m and 2200 m, respectively) and at a depth of 60, 70 and 80 m. For reference, a scheme of the testbed and the sea trials location is depicted in Figure 1. The three transmitters have been labeled T1 (1500 m from the VA, depth 60 m), T2 (2200 m from the VA, depth 70 m) and T3 (700 m from the VA, depth 80 m). The hydrophones of the VA have been dubbed H1, H2 and H4,[3] and are placed at 20, 40 and 80 m, respectively.

This configuration was specifically set up to study the behavior of the acoustic channel both when signals travel through the boundary between the mixed layer and the deeper layers, and when propagation takes place below the mixed layer. Oceanographic instrumentation, such as one Acoustic Doppler Current Profiler and one thermistor chain, was deployed close to the VA. The thermistor chain was designed for finer sampling in the mixed layer rather than in the lower layers, in order to better track temperature changes between 0 and 40 m of depth. The temperature samples gathered through the thermistors have been used to estimate the propagation speed of acoustic waves: previous studies on the physical features of the water in the Pianosa area showed that salinity is very stable over the whole summer season; therefore, frequent temperature measurements and a salinity measure taken once through a CTD (conductivity, temperature and density) sensor suffice to compute the sound speed profile (SSP) through the Mackenzie formula, e.g., see [10]. In Figure 2, we show the average value and the standard deviation of the measured sound speed at different depths in May, June and September. The figure allows to conclude that channel conditions were quite stable over time throughout the whole season, and that the general behavior of the channel was downward-refractive. As opposed to the stability of sound speed profiles, the roughness of the sea-surface greatly varied during the experiment period. The winds were typically calm, even though short periods with winds over 10 m/s were experienced. These winds generated local short-period waves that greatly affected sea surface roughness, ambient noise levels and sea surface reflections.

Of the many trials that have been performed over the summer, we will mainly focus on a representative subset including three experiments, each one lasting up to nine hours, that took place between May 30 and August 30, 2009.

III. Analysis of Impulse Channel Responses

We start by presenting the channel impulse response for transmissions carried out between any of the three transmitters and the deepest hydrophone, H4. Our technical report [11] presents a more extensive set of results including signals received at H1 and H2, which are omitted here for clarity. Experiments consist in the transmission of JANUS signals once every 30 seconds during a period of up to 9 hours. We

[2]We estimated the noise power spectral density in the 9–14 kHz band based on the same set of experiments considered in this paper, and found it to be approximately flat throughout the whole band.

[3]H3, placed at a depth of 60 m, experienced malfunctioning during the first of the three months of sea trials and died right thereafter. For this reason, we do not consider its recordings in our study.

recall that the JANUS version 0.0 signals we consider in this study are formed of three components: a sequence of wake-up tones, an HFM waveform sweeping the whole 9–14 kHz bandwidth, and a coded, FH-BFSK modulated data header plus an optional payload. For the moment, we concentrate on the HFM, whose narrow autocorrelation function allows a finely sampled estimation of the channel impulse response. The impulse response estimation is performed for each signal throughout the considered experiments, and the estimated functions are aligned with respect to the maximum amplitude arrival.

Figures 3, 4 and 5 show a pseudocolor plot of aligned channel impulse responses for the links T1–H4, T3–H4 and T2–H4, respectively. In each group of pictures, (a), (b) and (c) refer to the experiments which took place in May, June and August, respectively. The plots juxtapose consecutive channel realizations: the time at which the realization is measured is reported on the y-axis, whereas the x-axis shows the observation time within a single realization. (We recall that the zero time index represents the arrival epoch of the tap

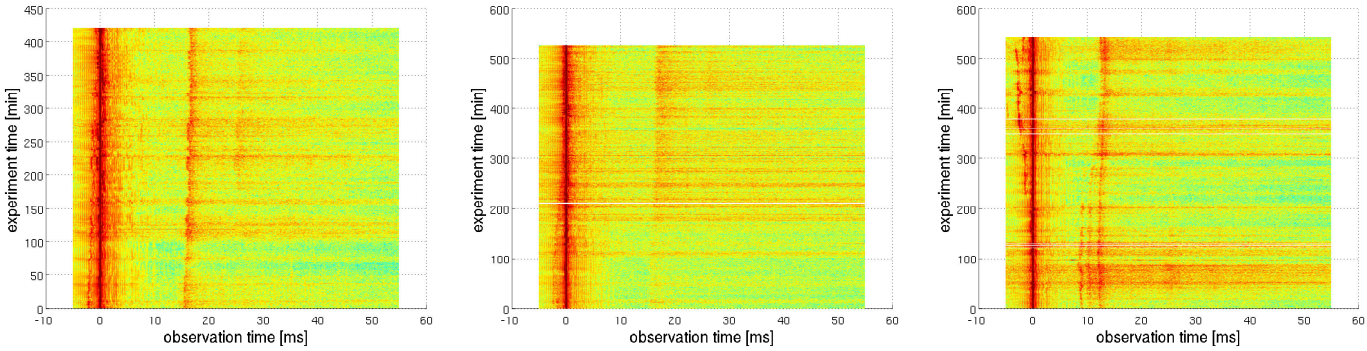

(a) Link T1–H4, May. (b) Link T1–H4, June. (c) Link T1–H4, August.

Figure 3. Pseudocolor plot of measured channel impulse response amplitudes for the link between T1 and H4.

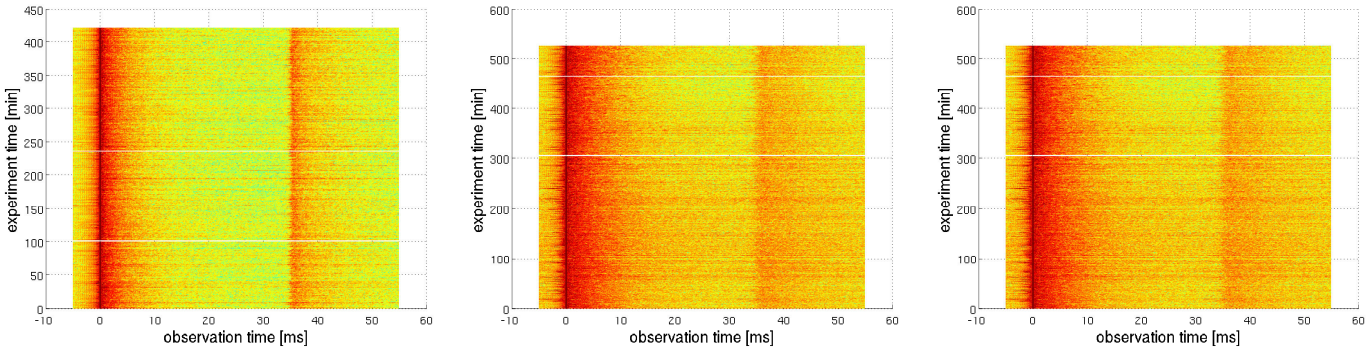

(a) Link T3–H4, May. (b) Link T3–H4, June. (c) Link T3–H4, August.

Figure 4. Pseudocolor plot of measured channel impulse response amplitudes for the link between T3 and H4.

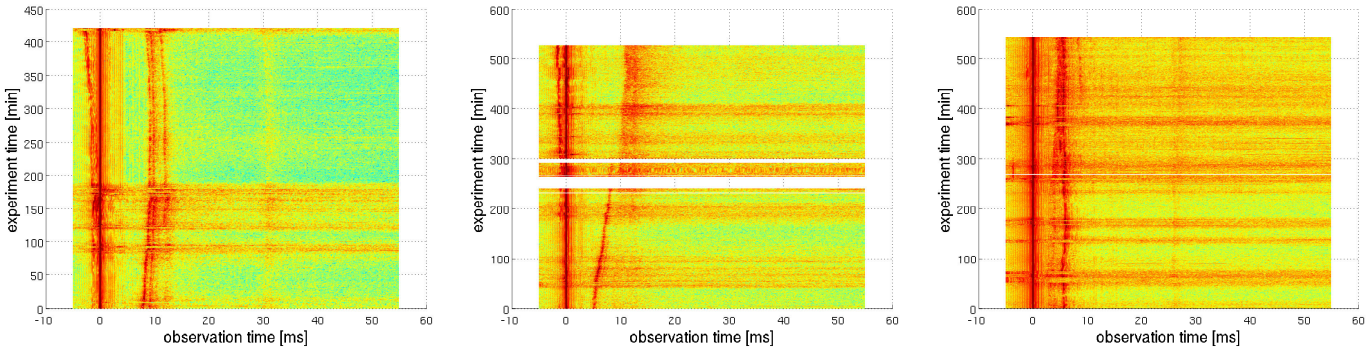

(a) Link T2–H4, May. (b) Link T2–H4, June. (c) Link T2–H4, August.

Figure 5. Pseudocolor plot of measured channel impulse response amplitudes for the link between T2 and H4.

of maximum amplitude.) Because significant contributions to multipath are bounded within the first tens of ms, the x-axis in the figures shows a time period from $-5\,\mathrm{ms}$ to $55\,\mathrm{ms}$. Given daily time constraints for the sea trials, the May experiment lasted 7 hours, whereas those in June and August lasted almost 9 hours.

Starting from Figures 3(a)–3(c), we can observe that link T1–H4 is quite stable: a second, faint arrival is found between 10 and $20\,\mathrm{ms}$, and a very strong main arrival is sometimes preceded by a smaller reflection. The same stability characterizes the T3–H4 link (see Figures 4(a)–4(c)). In this case the second, weaker arrival is between 30 and $40\,\mathrm{ms}$, while the spread of the main arrival is greater in June and August, because the warmer superficial waters created a more intense downward-refractive behavior. Unlike the T1–H4 and T3–H4 links, the T2–H4 link (Figures 5(a)–5(c)) is subject to slightly larger variability. Our interpretation in this case is that at close distance the direct and reflected paths incur similar attenuation, so that correlation is highly affected by small-scale phase changes. On the contrary, at larger distance propagation tends to take place along a dominating main path, which translates into a higher correlation.

Similar observations apply to the signals received at the other hydrophones, H1 and H2. By analyzing the data we can claim that channel paths are reasonably stable within the season, as we have shown for H4. For example channels T3–H2 and T3–H1 are characterized by a fixed number of arrivals (4 and 3, respectively), whose amplitudes and delays, relative to the main path, are fixed over the whole season. Signals from transmitters T1 and T2 show a slightly larger spread in time as we will discuss in the results for the delay spread.

A. Space-Time Channel Correlation

To better formalize the above observations, we derive the correlation coefficients between the channel realizations measured in each experiment (focusing again on the links between each of the three transmitters and H4). The correlation coefficient is estimated starting from channel response data sets such as those in Figures 3–5; given the set $\mathcal{C}_{t_0}^{\tau}$ of all pairs of responses separated by a time lapse of τ, starting from time t_0, we align these responses to the time of arrival of their respective maximum-amplitude taps, we compute the normalized correlation of signals within each pair, and finally take the average over all pairs in $\mathcal{C}_{t_0}^{\tau}$ as follows [1]

$$\rho(\tau) = \frac{1}{|\mathcal{C}_{t_0}^{\tau}|} \sum_{\mathcal{C}_{t_0}^{\tau}} \frac{\left| \sum_t g^*(t,t_0) g(t,t_0+\tau) \right|}{\sqrt{\sum_t |g(t,t_0)|^2 \sum_t |g(t,t_0+\tau)|^2}}, \quad (1)$$

where $g(t,t_0)$ and $g(t,t_0+\tau)$ are any two channel responses separated by a time lapse of τ, and $|\mathcal{C}_{t_0}^{\tau}|$ is the cardinality of the set containing such pairs. Given the experimental setup, the values of τ we can measure are integer multiples of $30\,\mathrm{s}$: for instance, for $\tau = 30\,\mathrm{s}$, we perform an ensemble average of the correlation coefficients between all signals transmitted at $(t_0, t_0+30\,\mathrm{s})$, $(t_0+30\,\mathrm{s}, t_0+60\,\mathrm{s})$, and so forth.

Figures 6–8 collect the correlation coefficients of the channel impulse responses as a function of the time displacement τ for the links between all transmitters and H4. The figures refer to the experiments carried out in May, June and August, respectively. The general behavior of the curves is to decrease to a fairly stable value, which depends on the day of the experiment and the transmitter-receiver pair. The rate of decrease towards the asymptotic value depends on distance, and is lower for short-distance links. It is interesting to observe that the correlation never approaches zero whatever large the considered time lapse may be, which is in accordance with other results such as those presented in [7]. The lowest floor value for the correlation is observed on the T3–H4 link, and can be explained by the quickly time-varying spread around the stronger arrivals. By defining the coherence time as the offset after which the correlation coefficient falls below some practical value (say, 0.8 [5]), we observe that the coherence time for these links depends on the day, in particular we note that within the inter-transmission time interval of $30\,\mathrm{s}$ the correlation of the T3–H4 channel falls quite abruptly, suggesting that the coherence time is indeed short; a higher rate of signal transmission would help estimate the actual coherence time with greater precision, and is left as a future direction of study. Conversely, the longer correlation times (and higher correlation floors) experienced on other links are due to the local stability of environmental parameters (such as bathymetry, sound speed profile, surface roughness and noise). The results for the channel coherence times are summarized in Table I.

We also performed a spatial correlation study in a similar way as reported before for time correlation: namely, we considered the channel responses to a single transmission as seen from the three hydrophones and computed their correlation; we then averaged over the set of all responses corresponding to the same vertical distance between the receivers. The results show nearly zero correlation between each pair of links. This lack of correlation can be justified by the very different propagation conditions experiences at different depths: while the downward-refractive behavior of the channel tends to bend signals toward the bottom and scatter them, H1 and H2 receive significant power from both the main propagation path and surface reflections, whereas H4 receives a strong direct path and very attenuated surface reflections, resulting in a more stable channel behavior.

Table I
COHERENCE TIME FOR LINKS T1–H4, T2–H4 AND T3–H4 ON MAY, JUNE AND AUGUST.

Month	T1–H4	T2–H4	T3–H4
May	$210\,\mathrm{s}$	$120\,\mathrm{s}$	$< 30\,\mathrm{s}$
June	$90\,\mathrm{s}$	$30\,\mathrm{s}$	$< 30\,\mathrm{s}$
Aug	$120\,\mathrm{s}$	$90\,\mathrm{s}$	$< 30\,\mathrm{s}$

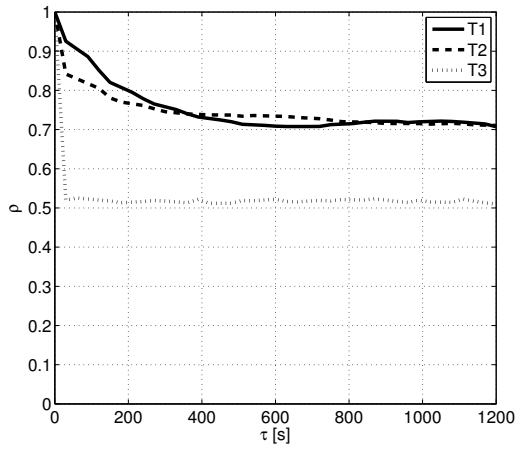

Figure 6. Channel correlation coefficient ρ as a function of time lapse τ in May. The links considered are from each transmitter T1, T2, T3 to hydrophone H4.

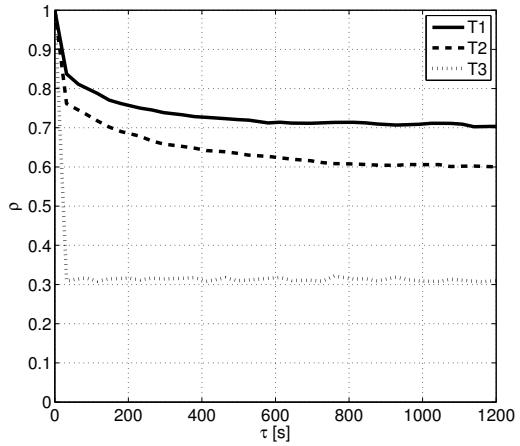

Figure 7. Channel correlation coefficient ρ as a function of time lapse τ in June. The links considered are from each transmitter T1, T2, T3 to hydrophone H4.

B. Power-Delay Profile

The analysis of the channel impulse responses also allows to gather an estimate of the channel time spread, which is required for tuning the parameters of adaptive signal processing algorithms at the receiver. The channel time spread can be inferred from the power-delay profile (PDP), i.e., the square value of the amplitude of the channel impulse response. In this section we will consider arrivals spaced by at least $2\,\mathrm{ms}$ and carrying at least 1% of the energy of the peak arrival. All PDPs are normalized to their peak value and aligned to the time of the strongest arrival The measured values for all links in May, June and August are summarized in Tables II, III and IV, respectively. From these values, we observe that the magnitude of the time spread is fairly stable throughout the season for all transmitter-receiver pairs, except T1–H4 and T3–H4, for which the variability is larger.

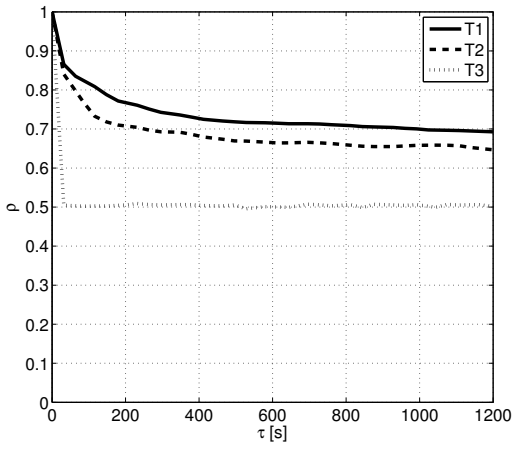

Figure 8. Channel correlation coefficient ρ as a function of time lapse τ in August. The links considered are from each transmitter T1, T2, T3 to hydrophone H4.

Table II
MEASURED TIME SPREAD IN ms FOR ALL LINKS IN MAY.

tx/rx	T1	T2	T3
H1	22	10	~ 0
H2	16	15	8
H4	~ 0	20	~ 0

Table III
MEASURED TIME SPREAD IN ms FOR ALL LINKS IN JUNE.

tx/rx	T1	T2	T3
H1	20	20	3
H2	18	22	5
H4	~ 0	15	10

Table IV
MEASURED TIME SPREAD IN ms FOR ALL LINKS IN AUGUST.

tx/rx	T1	T2	T3
H1	20	22	~ 0
H2	20	15	5
H4	14	14	8

In fact, H4 is influenced by whether or not reflections from the surface reach the sea bottom with significant power. While such reflections certainly affect H2, placed amidst the water column at a depth of $40\,\mathrm{m}$, they may or may not reach H4 depending on the time of the year, and the intensity of downward refraction. This is exemplified by Figures 9 and 10, plotting the significant arrivals of the channel for links T1–H4 and T1–H2. Both refer to the May experiment. In Figure 9 the channel has an impulsive behavior, and can therefore be modeled as ideal; recall that our model estimates the channel response by neglecting all taps bearing less than 1% of the energy of the maximum-amplitude tap: therefore, we infer that the T1–H4 channel is certainly characterized by

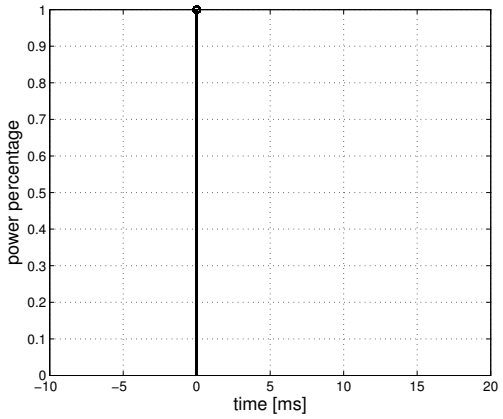

Figure 9. Normalized power delay profiles during May. The transmitter is T1, the receiver is H4.

a floor of secondary arrivals, but these arrivals bear negligible energy, allowing to simplify the channel response as a single impulse. On the contrary Figure 10 shows that the same signal is received at H2 with a much larger time spread, due to surface reflections. Since the power-delay profiles of channel realizations obtained in June and August are subject to similar observation as for the May realizations discussed here, they are omitted for brevity.

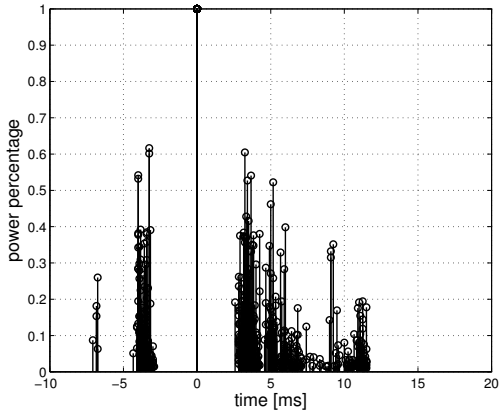

Figure 10. Normalized power delay profiles during May. The transmitter is T1, the receiver is H2.

C. Comparison against Bellhop simulations and discussion on network modeling

Given the recent interest in incorporating software to compute acoustic propagation into underwater network simulators [12], [13], in this section we elaborate on the accuracy of this approach in reproducing actual propagation conditions. Our aim is to show that even some limited environmental knowledge based on data collected during the experiment (in terms of bathymetry and temperature in the water column near the receiver) can be sufficient to reproduce statistically similar channel conditions through some ray-tracing simulation tools (we use Bellhop [8] in this paper). Indeed environmental sampling is not suitable for a "perfect" reproduction of propagation effects: temperature is only available in waters close to the receiver, salinity is approximated as constant throughout the season, bathymetry was sampled with a fine but still limited resolution, and in any event it is not feasible to run Bellhop using the large number of rays required so that fine-grained bathymetry data can be fully exploited. However, we argue that our limited environmental sampling still provides profitable results. We recall that such results are specific to the shallow water summer scenario considered here and to the signals in the 9–$14\,\mathrm{kHz}$ band: the same accordance should be proven for different central frequencies, where such environmental properties as water density discontinuities and surface roughness may have a different impact on the resulting channel impulse responses [14].

The propagation pattern predicted using the Bellhop tool can be found in Figures 11 through 13, which refer to the T1–H4 link (Figures 11(a) and 11(b)), the T3–H4 link (Figures 12(a) and 12(b)) and the T2–H4 link (Figures 13(a) and 13(b)). Only the experiments in May and June are shown, due to a malfunctioning in the thermistor chain which prevented data collection during part of August, including the experiment on August 30. By comparing these figures with the results obtained from the recorded traces (Figures 3(a) to 5(c)), we observe that the time spread predicted by the ray tracing program appears to be larger than inferred from experimental data. Furthermore, comparing Figure 3(a) against Figure 11(a) we note that the second arrival in Figure 3(a) is well predicted by Bellhop in the interval between 10 and $20\,\mathrm{ms}$, but its amplitude is greater than the measured second arrival. Moreover, Figure 11(a) shows other arrivals which do not actually occur. However, we are not seeking a completely accurate reproduction of all propagation effects, but rather a general representation with similar statistical properties. In particular, in the cases shown here a larger channel time spread means that the network simulator will model transmissions as taking place on a slightly worse channel than would be experienced in a real scenario, and therefore obtain a slightly conservative estimate of the transmission performance.

To complete the comparison among measured and Bellhop-predicted signals, we report in Figures 14–15 the time correlation of the channel responses as a function of the time lapse τ which is an integer multiple of $120\,\mathrm{s}$, since temperature was sampled once every two minutes. Compared to Figures 6–7, we can note that in simulated and measured data the correlation coefficients for both T1 and T2, though numerically different, show similar trends. A different behavior is observed for link T3–H4, for which the correlation coefficient is significantly overestimated in the simulations, which results in a reversed ordering of the curves compared to what reported in Figures 6 and 7.

IV. Communications performance

While the channel-related metrics discussed so far allow a direct comparison between measured and simulated channel

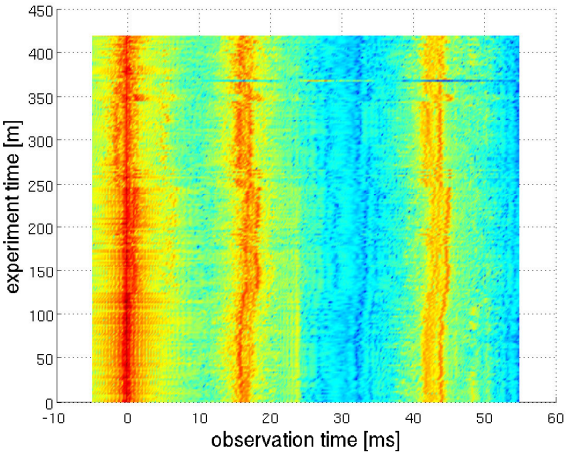

(a) Link T1–H4, May.

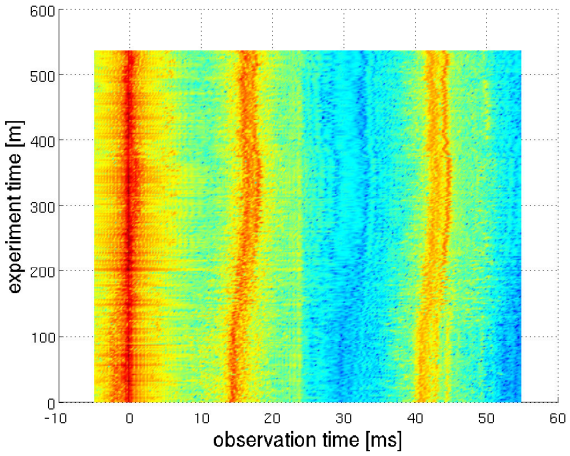

(b) Link T1–H4, June.

Figure 11. Pseudocolor plot of channel impulse response amplitudes simulated using Bellhop for the link between T1 and H4.

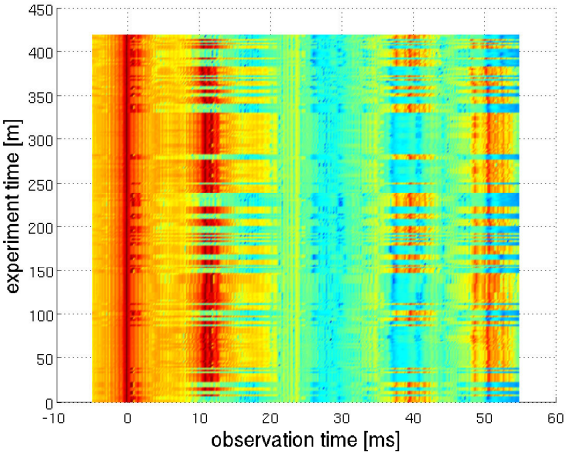

(a) Link T3–H4, May.

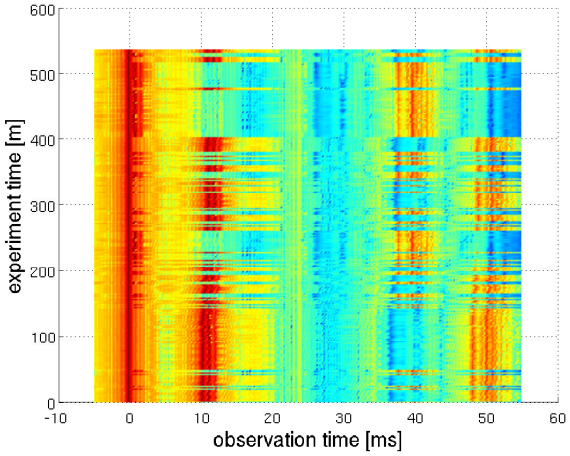

(b) Link T3–H4, June.

Figure 12. Pseudocolor plot of channel impulse response amplitudes simulated using Bellhop for the link between T3 and H4.

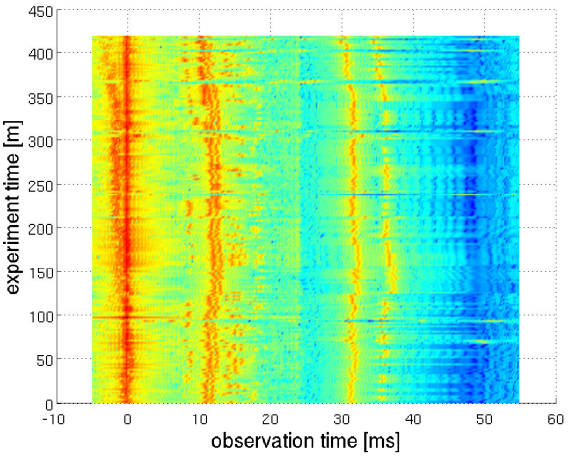

(a) Link T2–H4, May.

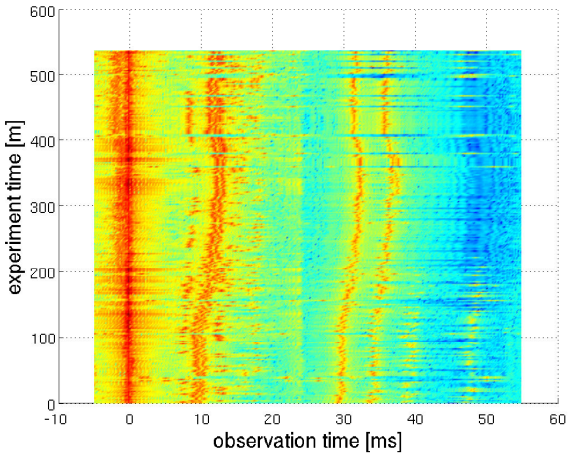

(b) Link T2–H4, June.

Figure 13. Pseudocolor plot of channel impulse response amplitudes simulated using Bellhop for the link between T2 and H4.

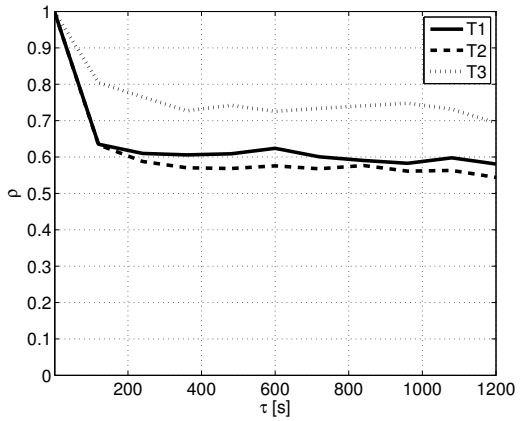

Figure 14. Channel correlation coefficient ρ as a function of time lapse τ in May predicted by Bellhop. The links considered are from each transmitter T1, T2, T3 to hydrophone H4.

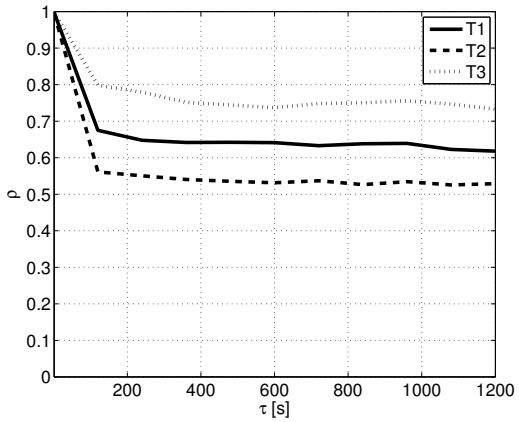

Figure 15. Channel correlation coefficient ρ as a function of time lapse τ in June predicted by Bellhop. The links considered are from each transmitter T1, T2, T3 to hydrophone H4.

behaviors, they can be translated into derived metrics that are, however, more directly tied to the performance evaluation of underwater acoustic networks. For example a model of space-time channel correlation may be used to predict the channel changes as nodes move. While uncorrelated behaviors are very frequently assumed for practical reasons, more extensive studies are required to understand in which cases this assumption actually holds. The channel outage probability, i.e., the probability that a time-varying channel does not deliver enough power to allow successful signal reception is a key metric for the performance evaluation of a mobile network. While the performance of a communication system given a certain channel behavior depends mainly on choices such as the signal modulation format, the type of signal processing at the receiver, and so forth, high-level channel characterization in terms of correlation and time spread is useful to drive system choices. These choices affect other measures such as the average coverage range experienced by a transmission, i.e., the distance at which the average received power is high enough to assume that incoming transmissions would be correctly received. Understanding the impact of channel behavior is therefore instrumental for the development of models that, though simple, would still reproduce network behavior at a sufficient level of accuracy for system design. In order to give an example of the above concept, we simulated the FH-BFSK modulation used in JANUS [3] over a channel modeled as is typically done in classic communications theory, i.e., as a tapped delay line, where the delay spread of the channel taps is chosen in accordance to experimental findings. The amplitude of the filter taps making up the modeled impulse response is Rayleigh distributed. In accordance with the channel parameters observed in the sea trials, the channel profile is generated so that 95% of the overall power is found within one up to three JANUS FH-BFSK symbols of duration $6.25\,\mathrm{ms}$ each: this corresponds to a time-spread ranging roughly from 6 to $20\,\mathrm{ms}$. Noise is then modeled as an additive white Gaussian process. Figures 16 and 17 compare the computed curves of Bit Error Rate (BER) as a function of SNR for different values of the time spread against measured BER samples, taken as the ratio of erroneous received bits over all sent bits in a given JANUS packet (made up of 144 bits); for each such packet, a marker is placed on either graph at the corresponding SNR-BER pair. For the purpose of representation in log scale, a custom constant value of 10^{-3} is added to all correct packets (which would show a BER of 0 otherwise). Figure 16 refers to a channel which can be modeled as impulsive (from T1 to H4). In this case, nearly 85% of all packets experience no errors. In addition, we observe that the SNR regime was particularly high (from 15 to $25\,\mathrm{dB}$) and the time spread of the channel is near 0 (ideal channel). Conversely, Figure 17 refers to a much more time-spread channel (from T2 to H2), where only 17% of all received packets are correct. All other measured BERs lie mostly between the curve for zero spread and the curve representing a spread of one to two FH-BFSK symbols (in May the time spread of the T2–H2 channel was $15\,\mathrm{ms}$ on average). It is interesting that the main reason for this behavior actually lies in the choice of the hopping pattern for the FH-BFSK modulation. The specifications of JANUS prescribe that such pattern be formed by sub-sampling a suitable Reed-Solomon codeword set so that the resulting codewords have desirable properties [3]: the direct consequence of one of these properties is that, out of the 144 bits making up a JANUS header, no more than 12 consecutive symbols happen to be transmitted on the same subcarrier; the same holds for symbols spaced 1, 2 or more symbol times. This implies that a channel with a limited time spread, spanning say 1 to 3 symbols, generates only limited inter-symbol interference. This explains why most measured BER points are found to be between the curve for zero spread and the curve for channel spread equal to one symbol time ($6.25\,\mathrm{ms}$) in either of the figures described above.

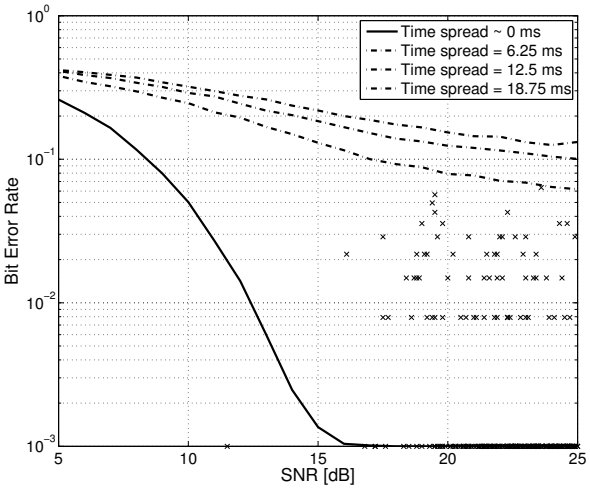

Figure 16. Comparison between analytically derived and measured BER as a function of SNR for the T1–H4 link in May, featuring an almost impulsive channel response.

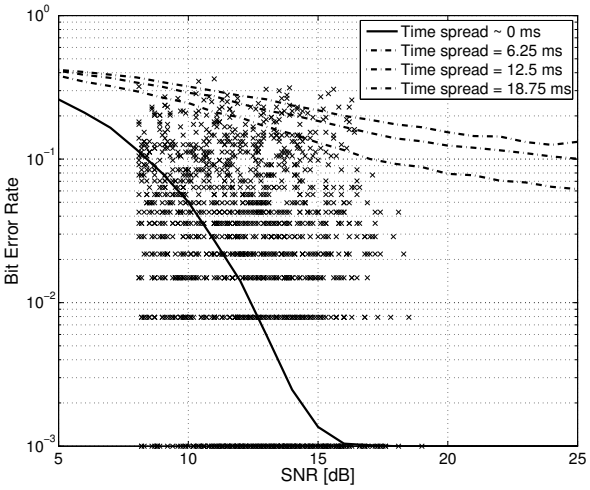

Figure 17. Comparison between analytically derived and measured BER as a function of SNR for the T2–H2 link in May, featuring a significantly spread channel response.

V. Conclusions

In this paper, we have presented an extensive analysis of channel properties in terms of time spread and correlation in time and space, carried out using the data from the SubNet 2009 sea trials. Our results show that the channel realizations tend to be correlated on the long term, and the level of correlation is distance-dependent. We also showed that negligible correlation is experienced between different hydrophones of the vertical array. We have also compared the results against those obtained through the Bellhop channel simulator and found that Bellhop tends to overestimate the channel time spread; we therefore argued that using Bellhop in network simulators would lead to a conservative estimate of the communication performance, due to the reproduction of conditions that are slightly worse than those found in practice in the considered environment and for the considered frequency band. As an example of comparison between measured and simulated network-relevant metrics, we studied bit error rate as a function of SNR for the JANUS modulation scheme, and found a reasonably good match.

Acknowledgment

This work has been supported in part by the NATO Undersea Research Centre under contracts no. 40800700 (ref. NURC-010-08) and 40900654.

References

[1] A. Radosevic and J. G. Proakis and M. Stojanovic, "Statistical Characterization and Capacity of Shallow Water Acoustic Channels," in *Proc. of IEEE OCEANS*, Bremen, May 2009.

[2] P. Qarabaqi and M. Stojanovic, "Statistical modeling of a shallow water acoustic communication channel," in *Proc. of IACM UAM*, Nafplion, Greece, Jun. 2009.

[3] K. McCoy, "JANUS: from primitive signal to orthodox networks," in *Proc. of IACM UAM*, Nafplion, Greece, Jun. 2009.

[4] P. L. Nielsen and M. Siderius and F. B. Jensen, "Acoustic time-variability measurements in the Straits of Sicily," in *Proc. of the European Conf. on Underwater Acoustics*, Lyon, France, Jul. 2000.

[5] T. C. Yang, "Measurements of temporal coherence of sound transmissions thorugh shallow water," *Journal of the Acoustic Society of America*, vol. 120, no. 5, pp. 2595–2614, Nov. 2006.

[6] ——, "Temporal coherence of sound transmissions in deep water revisited," *Journal of the Acoustic Society of America*, vol. 124, no. 1, pp. 113–127, Jul. 2008.

[7] A. G. Zajic, "Statistical space-time-frequency characterization of MIMO shallow water acoustic channels," in *Proc. of IEEE OCEANS*, Biloxi, Oct. 2009.

[8] M. Porter *et al.*, "Bellhop code." [Online]. Available: http://oalib.hlsresearch.com/Rays/index.html

[9] "Teledyne benthos undersea systems and equipment," www.benthos.com.

[10] Woods Hole Oceanographic Institution, "Ocean Toolbox." [Online]. Available: ftp://acoustics.whoi.edu/pub/Matlab/oceans/

[11] B. Tomasi, P. Casari, M. Zorzi, G. Zappa, and K. McCoy, "Experimental study of the acoustic channel properties during subnet 2009," University of Padova, Tech. Rep., 2010. [Online]. Available: http://telecom.dei.unipd.it/pages/read/75/

[12] F. Guerra, P. Casari, and M. Zorzi, "World Ocean Simulation System (WOSS): a simulation tool for underwater networks with realistic propagation modeling," in *Proc. of WUWNet 2009*, Berkeley, CA, Nov. 2009.

[13] N. Parrish, L. Tracy, S. Roy, P. Arabshahi, and W. Fox, "System design considerations for undersea networks: link and multiple access protocols," *IEEE J. Select. Areas Commun.*, vol. 26, no. 9, pp. 1720–1730, Dec. 2008.

[14] F. Jensen, W. Kuperman, M. Porter, and H. Schmidt, *Computational Ocean Acoustics*, 2nd ed. New York: Springer-Verlag, 1984, 2nd printing 2000.